Effect of TiO2 and 11 minor elements on the reactivity of ground-granulated blast-furnace slag in blended cements

Simon Blotevogel, Laurent Steger, Daniel Hart, Lola Doussang, Judit Kaknics, Mathilde Poirier, Hansjörg Bornhöft, Joachim Deubener, Cédric Patapy, Martin Cyr

Effect of TiO_2 and 10 minor elements on the reactivity of ground granulated blast furnace slag (GGBS) in blended cements

Simon Blotevogel[1,*], Laurent Steger[1,2], Daniel Hart[4], Lola Doussang[2], Judit Kaknics[3], Mathilde Poirier[2], Hansjörg Bornhöft[4], Joachim Deubener[4], Cedric Patapy[1], Martin Cyr[1]

[1] *LMDC, Université de Toulouse, INSA/UPS Génie Civil, 135 Avenue de Rangueil, 31077, Toulouse cedex 04, France*

[2] *Ecocem Materials, 324061, Block F1, Eastpoint Business Park, Dublin 3, Ireland*

[3] *ArcelorMittal Maizieres Research, Voie Romaine, 57283 Maizières-les-Metz, France*

[4] *Institute of Non-Metallic Materials, Clausthal University of Technology, Germany*

**Simon.Blotevogel@insa-toulouse.fr*

Abstract

Ground granulated blast furnace slags (GGBS) are glasses (>99%) of the CaO-Al_2O_3-SiO_2 compositional system and are widely used as supplementary cementitious materials. Differences in reactivity of GGBS were screened by modifying the content of 11 minor elements (namely Ba, Ce, Cs, Cr, Mn, P, Sn, Sr, Ti, V, Zr). SEM observations showed that most elements entered the silicate glass matrix, only Sn was reduced to its metallic form and P accumulated in minor minerals. Mortar strength tests showed that 2d-compressive strength was reduced by > 50% for a TiO_2 content of 2.5 wt.% in the slag. At 28 days the loss in compressive strength was still > 40%. Calorimetric tests on other element additions showed that network modifiers (Ba, Cs and Sr) and GGBS reactivity are positively correlated, whereas Ce, Cr, V and Zr significantly decreased reactivity. It is shown that these effects can be well estimated by the weighted field strength of the added element.

Keywords: blast furnace slag (GBFS), minor elements, field strength, R3-test, titanium dioxide, supplementary cementitious materials

This article was published on the 1st of September 2020 under DOI: 10.1111/jace.17431 in the Journal of the American Ceramic Society.

1. Introduction

Ground granulated blast furnace slags (GGBS) are by-products of the pig iron production and have been used as a cement additive for almost 150 years [1, 2]. GGBS is a common constituent in CEM II and CEM III (EN 197-1), replacing clinker/Portland cement up to 95% in some applications. GGBS-containing binders have superior long term properties, including increased chemical and mechanical resistance and decrease the CO_2 footprint of the material [2–7]. Starting from a certain addition level, early compressive strength development is below the ordinary Portland cement (OPC) or cements with lower additions levels [2, 3, 6].

However, large differences exist in short term reactivity of GGBS. It was shown that in different modern day GGBS, 2d compressive strength in mortars with 75 % GGBS varied by a factor x4 [8]. Main source of variation of the reactivity of GGBS in various cementitious systems was their chemical composition and intensive research has been carried out on the influence of major element composition [8–15]. Differences in reactivity are likely due to differences in chemical durability of the slag glass, as for strength development GGBS needs to dissolve and reprecipitate as cementitious phases [6].

Chemically, GGBS are glasses (>99%) of the CaO-Al_2O_3-SiO_2 compositional system, also containing significant amounts of Mg and Ti, and a wide variety of other minor and trace elements [2, 6, 16]. Structurally, main network formers are Si and the majority of Al, as often observed in calcium aluminosilicate glasses [16–18]. Ca and Mg are present in network modifier positions [16].

Various minor and trace elements are present in GGBS and their mobility from slag have been studied for environmental reasons [19, 20]. In a survey of a large variety of American GGBS, Ba, Be, C, Cr(III), Fe, Mg, Mn, S, V and Zn were found in all GGBS [20]. Mean

concentrations of these elements ranged from 8.2 mg/kg for Be to 17 g/kg of Fe. Furthermore, As, Co, Cu, Pb, Mo, Ni, P, Se and Sn were detected in some of the slags [20]. Proctor et al. (2000) stated that the metal leaching from blast furnace slags is low, arguing that the metals are directly included in the glass matrix [20]. Yet, little is known on the effect of those elements on GGBS reactivity in blended cements.

One minor element that has a known effect on GGBS reactivity is Ti. Its presence has been noted to have a negative effect starting from 1 wt.% TiO_2 in slags used in blended cements [12, 21, 22]. Wang et al. 2002 found that there was an almost linear effect of TiO_2 content on GGBS reactivity, with the exception of high alumina slags [22]. This study found a similar effect in blended cements and alkali activated materials, but Tänzer et al. 2015 showed that the effect of TiO_2 in alkali activated GGBS was negligible [13, 22]. This means that existing information are contradictory.

To our knowledge, the only other minor element investigated for its effect on GGBS reactivity was Mn. Péra et al., (1999), concluded that increasing MnO contents (5.4 – 21.0 wt.%) reduce compressive strength at 3d and 7d but increase compressive strength after 28d [23]. Metallurgical slags with high MnO concentrations (> 15 wt.%) were judged unsuitable for the use in blended cements [24]. Furthermore, Mn was investigated for its potential effect on steel corrosion in cementitious materials [25]. However, these studies were carried out using different initial slag compositions, most of them were very different from standard GGBS compositions.

The aim of this study was to provide experimental data on the effect of a variety of minor elements on GGBS reactivity in blended cements. Therefore, 11 elements were selected and added to a remelted industrial GGBS. Selected elements were chosen according to three

criteria. First, Ti, Cr, V and Mn were chosen because they are frequently encountered in industrial GGBS. The aim was to estimate their influence on GGBS reactivity. Second, large network modifying cations Cs, Ba, K, Sr were selected to evaluate if their presence would increase GGBS reactivity. The selection was based on earlier research that showed chemical durability increased in the order Mg > Ca > Sr > Ba for boro-aluminosilicate glasses, suggesting that increasing cation sizes may destabilize the glass [26–29]. And third Ce, P, Sn and Zr were added to the industrial slag as nucleating agent to test if phase separation and possibly perovskite precipitation could be initiated to increase GGBS reactivity [30–36].

In laboratory scale trials, around 100 g of an industrial GGBS modified by additions of one minor element at a time were produced. Amorphous state of resulting slags was checked by X-ray diffraction (XRD) and scanning electron microscopy (SEM) and composition by X-ray fluorescence (XRF). Slag reactivity was then screened using a modified calorimetric R3 protocol [8, 37]. This test is based on a model system approach that imitates concrete pore solution using only pure components [37, 38]. To validate the calorimetric protocol 4 different levels of Ti modified slags were prepared and their compressive strength tested on 2 x 2 x 2 cm^3 mortar cubes.

2. Materials and Methods

2.1 Sample preparation

All prepared glasses were based on the same industrial blast furnace slag (GGBS), which was mixed with the different additives (Table 1). Minor elements were added as their respective stable oxides, exceptions were P, K and Cs. Phosphorus was added as calcium phosphate,

potassium and cesium were used in their carbonate forms. Added minerals were purchased from Alfa Aeser, Prolabo, Rectapur and VWR, their purity was >98 % (m/m).

Concentrations of TiO_2 additions were chosen to reflect contents of modern day GGBS (0.2 – 3.0 wt.%) [8, 39]. MnO additions were set to 3 wt.%, V_2O_5 and Cr_2O_3 to about 1 wt.%, which were our estimates for maximum concentration that could occur in a modern industrial setting. Network modifier additions of Sr and Ba were chosen to be close to 2 wt.%, a compromise between economic viability for a potential application on industrial scale and amount necessary to observe an effect. Concentrations of Cs and K concentrations were even lower due to volatilization of alkaline elements during the remelting process. ZrO_2 addition was set to be 5 wt.% according to earlier observations on nucleation of GGBS [30]. Only few data is available for the other nucleating agents in GGBS like glasses so that concentrations were set arbitrarily to 2 wt.% for CeO_2 and to 1 wt.% for SnO_2 and P_2O_5.

Table 1. Desired concentrations and compounds used for minor element additions.

Element	Used compound	Desired concentration wt.% (oxide)
Cs	Cs_2CO_3	0.9
V	V_2O_5	1
Cr	Cr_2O_3	1
Sn	SnO_2	1
P	$Ca_3(PO_4)_2$	1
K	K_2CO_3	1.4
Sr	SrO	2
Ba	BaO	2
Ce	CeO_2	2
Ti	TiO_2	0.6-2.5
Mn	MnO	3
Zr	ZrO_2	5

Fixed compositions of the samples were placed in a graphite crucible in a Nabertherm HT16/17 furnace preheated to 1600 °C for 5 minutes. Short processing times are possible due to the low viscosity of GGBS glasses at 1600°C of about 1 Pa.s (10 times lower than that of soda-lime-silica glass) and the fact that the main component was already provided as a glass [40, 41]. The furnace was purged with argon to limit interaction of air with the graphite crucible. The samples were taken out of the furnace at 1600 °C with a pair of pliers and quenched in a laboratory scale granulation device using pressurized water flow. The recovered granulated slag was dried overnight at 110 °C. To account for the different quenching conditions between laboratory and steel industry, the industrial GBS (without additions) was also remelted and used as reference.

Final compositions and amorphous state were checked by XRF and XRD, respectively. The resulting fritted granules were then ground using a Retsch RS100 disc mill (15 g of slag in a 50 mL tungsten carbide bowl for 1 min at 1400 rpm) to give about 4200 cm^2/g Blaine fineness [8].

XRF measurements were carried out on a S8 Tiger device by Brucker. The samples were prepared using a mix of lithium meta- and tetraborate, results are displayed in Table 2. XRD scans were carried out on disoriented powder samples on a Brucker D8 device, using a Cu-anticathode. Scan duration was 65 min for angles from 5 to 70° and air scattering was reduced by using a beam knife. During measurement, the samples were spun around the vertical axis to improve particle statistics. XRD patterns are displayed in Figure 1. All modified GGBS were amorphous with exception of the SnO_2 modified slag, which showed characteristic peaks for metallic Sn(0). Note that XRD does not rule out small fractions of crystals not detected by this method.

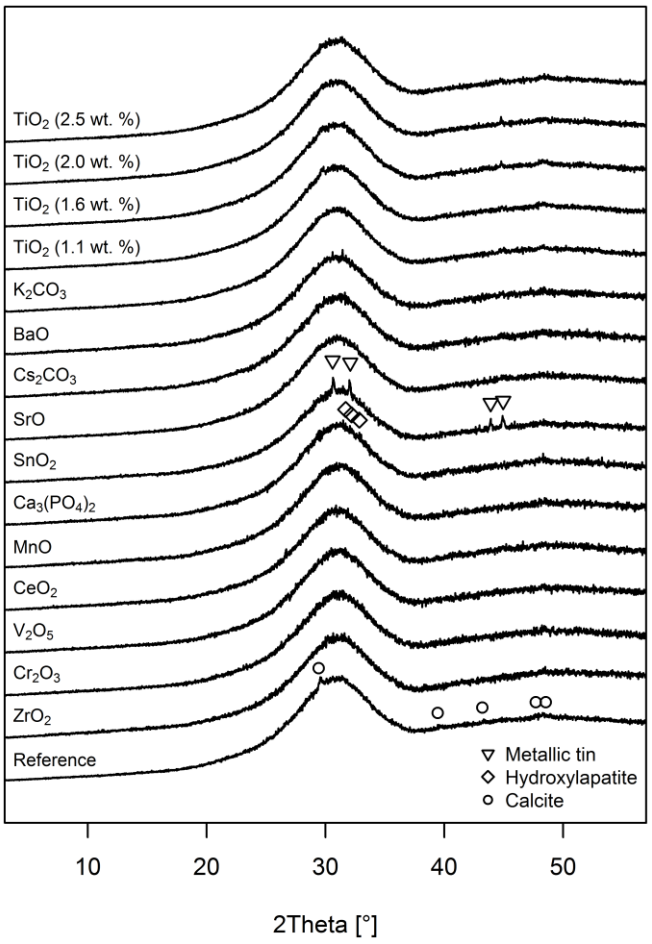

Figure 1. XRD patterns of modified and base GGBS (reference) for comparison. Slags are mainly amorphous with only minor peaks visible for some additions. The peaks in the sample with SnO_2 addition can be assigned to metallic tin (triangles). In the reference sample peaks correspond to calcite, indicating the onset of carbonation. In the sample with $Ca_3(PO_4)_2$ addition there is some noise in the range of the main hydroxylapatite that might indicate the minor presence of the mineral, but intensity is too low for unambiguous attribution. Peaks around 30° in the sample with BaO addition correspond to various Fe-Ba-oxides, and minor peaks around 45° in samples with TiO_2 additions correspond to Fe-alloys of different stoichiometry. The absences of secondary peaks make it difficult to unambiguously identify those phases.

2.2 Compressive strength tests

Compressive strength tests were carried out on 2 cm x 2 cm x 2 cm mortar cubes, using Ti-modified GGBS. The mortar was prepared using 75 wt.% GGBS and 25 wt.% cement, based on EN 196-1 for normalized mortars. A batch of mortar contained one part by mass of binder (75 wt.% GGBS and 25 wt.% cement), three parts by mass of sand and one-half part of water (water/binder ratio 0.50). Mortars were mixed using a normalized Automix 65-L0006/A mixer, following the speed and time of mixing recommended by EN 196-1. The cement was made of clinker and gypsum addition (4.1 wt.% SO_3). The samples were stored at 20 °C and 50% relative humidity for 24 h. Subsequently, the cubes were transferred into hermetic bags until compressive strength testing. Six cubes were tested for each age (1 day, 2 days and 28 days), using an IGM machine. Measured values are reported as the mean compressive strength of six cubes and measurement error is given as 95 % confidence interval.

2.3 Isothermal calorimetry

All calorimetric tests were carried out using TAM Air isothermal calorimeter by TA-instruments, operated at 40 °C. Details of the method were published elsewhere [8]. In brief, 1.5 g of GGBS together with 4.5 g of laboratory grade $Ca(OH)_2$ were placed in a polypropylene recipient. Then a solution of 0.3 M K (from KOH and K_2SO_4 (1 : 5 w/w)) was added in a s/l ratio of 0.8. The pastes were hand stirred using a glass bar until no agglomerates or layering was visible anymore. Finally, 8.5 g of the pastes were transferred into a sealed measurement vessel, after 45 min equilibration period cumulative reaction heat was measured for 24 h.

2.4 SEM observations

The morphology characteristics of unground GGBS samples were analyzed by scanning electron microscopy (EVO50, Zeiss, Oberkochen). In order to obtain the SEM measurements, the samples were prepared in two ways. On the one hand, the surface of a grain was analyzed by gluing the grain on a sample holder and sputtered with gold. On the other hand, a GBS grain was embedded in resin to observe the inner structure of the grain. After hardening, the sample was polished and sputtered with gold.

Table 2. XRF analysis (wt.%) of reference and modified GGBS

GGBS	Al_2O_3	CaO	MgO	SiO_2	TiO_2	K_2O	ZrO_2	Cr_2O_3	V_2O_5	CeO_2	MnO	P_2O_5	SnO_2	SrO	Cs_2O	BaO
Reference	9.6	40.9	6.4	37.6	0.6	0.3										
Modifcations																
ZrO_2	9.4	39.9	6.6	36.4	0.6	0.3	5.1									
Cr_2O_3	9.7	41.8	6.7	37.5	0.6	0.3		1.3								
V_2O_5	9.7	42.1	6.8	37.5	0.6	0.3			0.9							
CeO_2	9.7	41.5	6.7	37.2	0.7	0.3				1.9						
MnO	9.5	41.4	6.7	37.1	0.6	0.3					2.9					
$Ca_3(PO_4)_2$	9.5	43.8	6.6	36.9	0.6	0.3						1.1				
SnO_2	9.8	42.4	6.8	37.9	0.7	0.3							1.2			
SrO	9.7	41.6	6.7	37.4	0.6	0.3								1.8		
Cs_2CO_3	9.9	42.4	6.9	38.0	0.7	0.3									0.2	
BaO	9.6	41.7	6.7	37.2	0.7	0.3										2.0
K_2CO_3	9.8	42.1	6.8	37.8	0.7	1.2										
TiO_2 (1.1)	9.8	42.6	6.8	38.1	1.1	0.3										
TiO_2 (1.6)	9.7	42.4	6.8	37.8	1.6	0.3										
TiO_2 (2.0)	9.7	42.1	6.8	37.7	2.0	0.3										
TiO_2 (2.5)	9.7	41.9	6.8	37.4	2.5	0.3										

3. Results

3.1 Compressive strength tests

Compressive strength test on 2 x 2 x 2 cm^3 mortar cubes are reported in Figure 2. For the GGBS samples containing up to 2.0 wt.% of TiO_2, no significant difference is observed after 1 d of curing. Compressive strength is between 1.7 and 1.9 MPa for these samples. Only the sample containing the GGBS with 2.5 wt.% of TiO_2 has significantly lower compressive strength (1.3 MPa) at 1 d.

After 2 d, compressive strength declines from 4.9 MPa, for the reference slag containing 0.6 wt.% TiO_2 to 1.9 MPa for the slag with the highest TiO_2 content (2.5 wt.%) (Figure 2). The decrease in compressive strength is proportional to the increasing TiO_2 content. For the sample with the highest TiO_2 content, corresponding to 1.9 wt.% more TiO_2 than the reference, compressive strength is > 50% lower than for the reference samples. After 28 d there is still a significant decrease of compressive strength with increasing TiO_2 content. Compressive strength is between 31.7 and 17.7 MPa, for the above-mentioned highest and lowest TiO_2 levels in GGBS (Figure 2). This represents a relative decrease of > 40% in compressive strength for the sample with the highest TiO_2 addition with respect to the reference, slightly less than for the 2 d samples. The decrease appears to be also proportional to the increase in TiO_2.

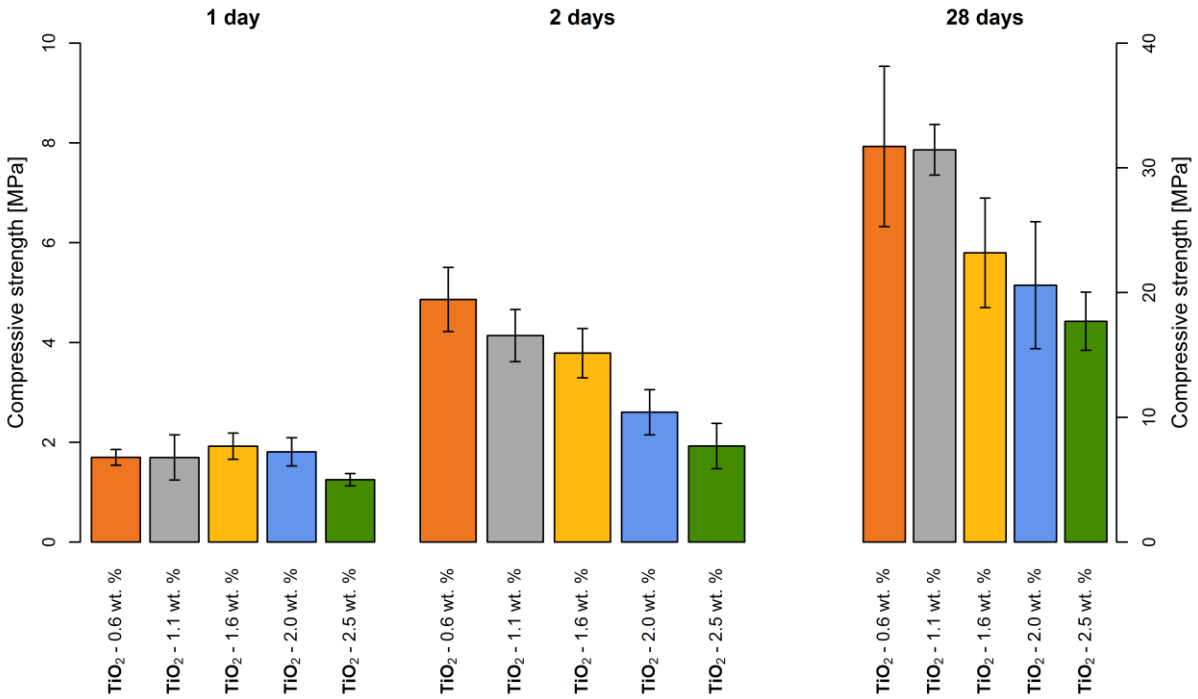

Figure 2. Compressive strength of standard mortars (75 wt.% GGBS and 25 wt.% cement) using GGBS with different TiO_2 contents. Error bars are 95% confidence intervals calculated from 6 replicates. Note that the ordinate axis has different scales, on the left for 1 and 2 days, and on the right for 28 days.

3.2 Calorimetric measurements

Calorimetric tests showed decreasing heat values with increasing TiO_2 content (Figure 3). The measured values were reported in Table 3. The heat values correlated well with compressive strength tests on 75% GGBS mortars (Figure 3). Pearson's R^2 was 0.91 for the correlation between 2 d compressive strength and R3-heat and 0.92 for 28 d strength and 24 h heat.

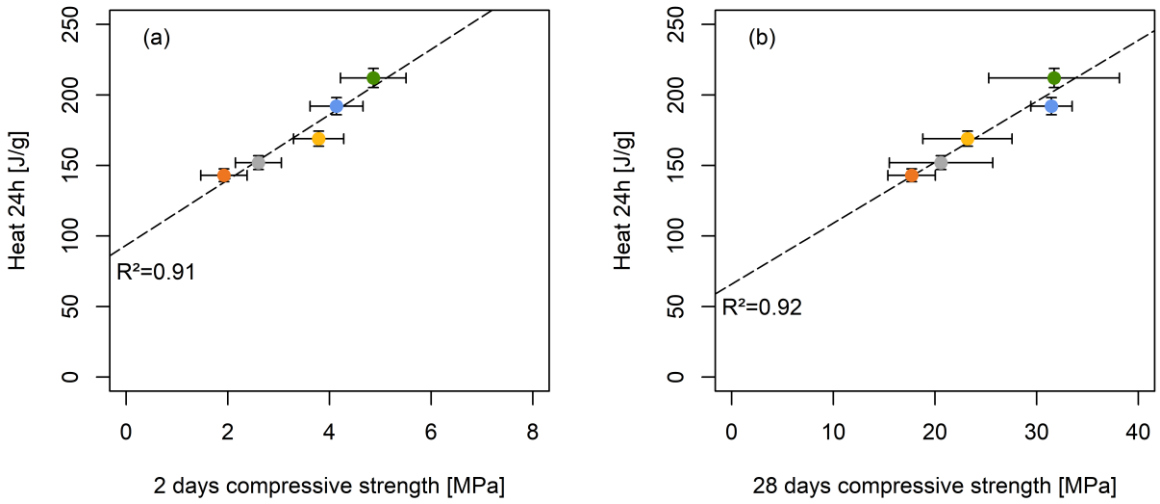

Figure 3. Heat development during R3 test of reference and TiO_2 modified GGBS plotted against compressive strength of standard mortar pastes after (a) 2 days of curing and (b) 28 days of curing. The dotted line is a linear regression, corresponding R^2 value as indicated. Horizontal error bars are 95% confidence intervals calculated from 6 replicates and vertical error bars correspond to 2RSD interval of the method [8].

For the modification trials using other elements than Ti, heat values are displayed in Figure 4. Heat release of the highest TiO_2 addition is also included in the Figure. Addition of 5.0 wt.% ZrO_2 gave the least reactive experimental GGBS with a heat release of only 104 J/g, less than half as much as the reference sample. Additions of Cr_2O_3 (1.3 wt.%), V_2O_5 (0.9 wt.%) and CeO_2 had similar negative effects on GGBS reactivity (168, 169 and 178 J/g, respectively). MnO and P_2O_5 additions appear to have slight negative effects on GGBS reactivity. Please note that Ca was also added through $Ca_3(PO_4)_2$ additions giving the sample with the highest CaO content. However, when a 2xRSD range is considered as the method error, ranges from the latter two samples and the reference overlap [8]. Additions of SnO_2 (1.2 wt.%), SrO (1.8 wt.%), Cs_2O (0.2 wt.%) and BaO (2.0 wt.%) had slight positive effects on GGBS

reactivity but were all within the 2xRSD range of the reference samples. The addition of 1.2 wt.% K_2O had a significant positive effect on GGBS reactivity with a heat release of 233 J/g.

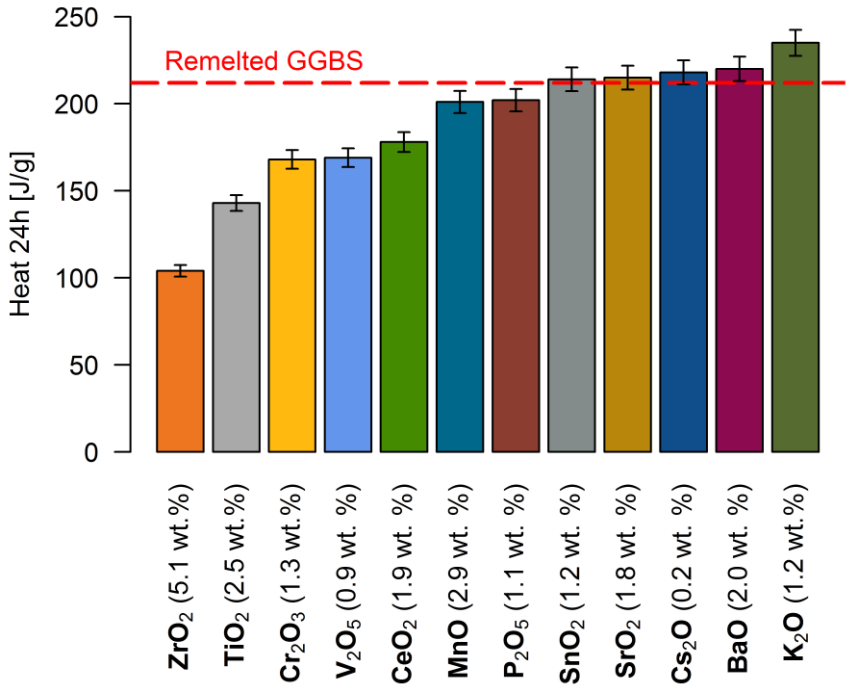

Figure 4. Heat development during R3-test of modified GGBS. Note that only the sample with the highest TiO_2 content is displayed. The red dotted line indicates heat development of unmodified remelted GGBS reference. Error bars correspond to 2RSD interval of the method [8].

3.3 SEM observations of selected GGBS samples

SEM observations of polished GGBS surfaces showed the presence of small (> 1 µm) metallic iron droplets in most samples. These droplets were enriched in Ce, Cr, Mn, P, Sn, Ti, V and Zr,

but most elements were also detected in the glass matrix. As the amount of iron in GGBS was very low (< 0.2 wt.% in XRF measurements), it was considered that the enrichment in metal droplets did not influence on overall glass concentration for most elements.

Only, Cs, Sn and P were not detected in the glass matrix by EDX. For Cs this is likely due to the fact that the amount added is lower than the EDS detection limit. For Sn, high concentrations in iron droplets and the formation of almost pure metallic Sn and Sn alloy droplets (Figure 5) indicate that, under the remelting conditions, Sn was reduced to its metallic state and did not dissolve in the glass matrix. This is confirmed by the presence of metallic tin peaks in the XRD pattern of the slag (Figure 1). P also showed high enrichment in metal droplets, and some apatite crystals were observed on the slag surface, so that it was assumed that P did not dissolve in the glass matrix either (Figure 6). XRD scans, however, did not show clear apatite peaks, likely because its presence remained below detection limit.

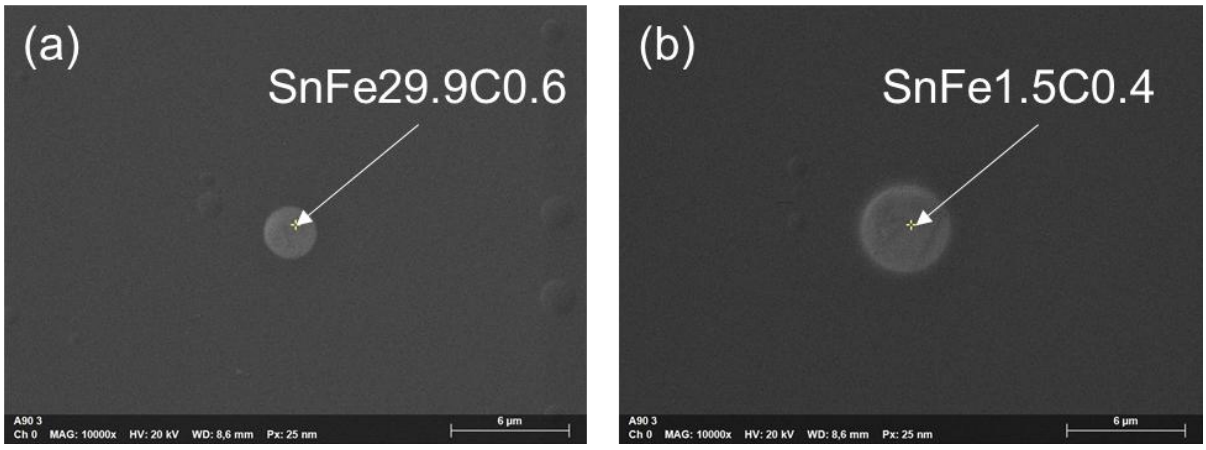

Figure 5. Secondary electron image of Sn-Fe alloy (a) and Sn droplets (b) in polished thin sections of the SnO_2 modified GGBS. Note that composition (EDX in wt.%) is indicated by assuming that all elements are alloying Sn.

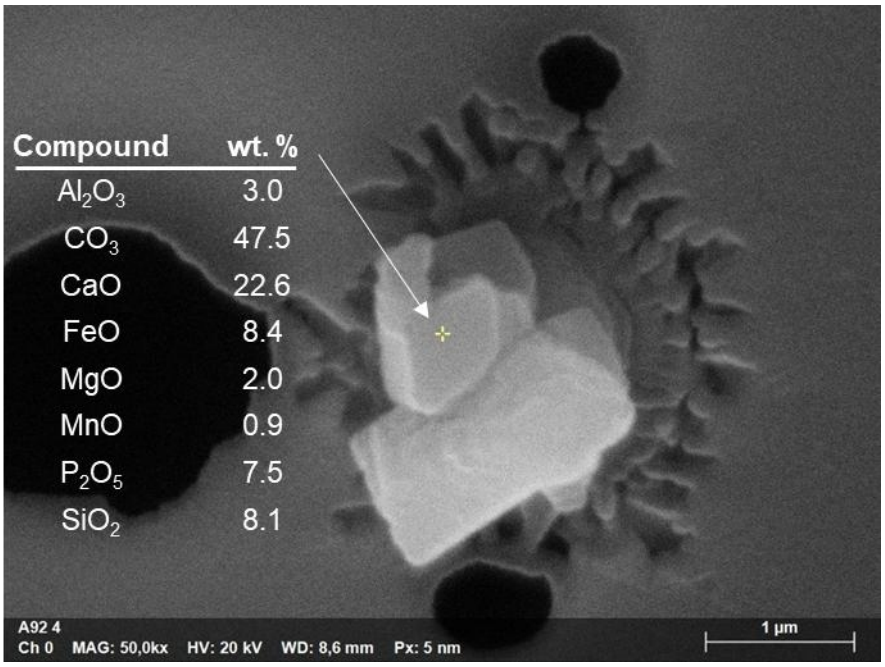

Figure 6. Apatite/carbonate crystals on the surface of the phosphorous modified GGBS sample.

4. Discussion

4.1 Influence of Ti on the reactivity of GGBS

TiO_2 additions had a strong negative effect on mortar compressive strength of 75 wt.% GGBS mortars at 2 d and 28 d. The sample with 2.5 wt.% of TiO_2, an addition of only 1.9 wt.% with respect to the reference industrial GGBS, lost > 50% of compressive strength with respect to the reference at 2 d, and still > 40% at 28 d. This is slightly more than reported by Wang et al., (2002) [22]. For 1 d samples, only the highest TiO_2 addition showed a significant loss of compressive strength while all other samples were within method error. This is likely due to the low contribution of GGBS to the hydration process during the first day. Indeed, it was shown that a significant contribution of GGBS to the hydration reaction is only detectable after about 12 h in blended cements [43].

Our observations confirm the negative effect of TiO_2 content on GGBS reactivity reported by Wang et al., (2002) [22]. It was also confirmed that the negative effect is proportional to the amount of TiO_2 added. This is in contrast to a study on alkali activated materials showing only a slight effect of TiO_2 content on GGBS reactivity [13]. As compressive strength is mainly due to C-S-H formation, the persistence of the effect in time suggests that TiO_2 affects the reaction of Ca and Si necessary for their formation, possibly by slowing down GGBS dissolution. A constant decreased dissolution rate would also explain the correlation between R3-heat and 28 d compressive strength. Indeed, a former study on different GGBS found good correlation only for R3 heat and 2 d strength, as compressive strength results converged at later ages [8].

The correlation between 2 d compressive strength and reaction heat during the R3-test was slightly better for the TiO_2 modified slags than reported for a set of 16 industrial GGBS [8]. This confirms that the R3 test is an appropriate tool to investigate the influence of minor elements on GGBS reactivity. In the following the R3 heat release was used as a proxy for compressive strength development of GGBS containing mortars.

Table 3. Coordination numbers, bond length and field strength of the added elements in GGBS like glasses, taken from literature. FSI index values were computed using this data. If, for a given element, multiple coordination sites were identified in the cited reference, the coordination noted in the table is the average coordination of the element rounded to the next natural number.

Addition	Charge	Coordination	R	Bond length	Source	Field strength	Conc. Added	Index value	Heat
	eq		Å	Å		eq/Å²	Mol % (Oxide)		J/g
ZrO_2	**4**	7	0.78	2.10	[44]	0.91	2.55	1.12	104
Cr_2O_3	**3**	6	0.62	1.97	[20, 45, 46]	0.78	0.51	0.32	168
V_2O_5	**4**	6	0.58	1.93	[45, 47]	1.07	0.30	0.52	169
CeO_2	**3**	6	1.01	2.36	[45, 48]	0.54	0.67	0.05	178
MnO	**2**			2.05	[49]	0.48	2.46	0.02	201
P_2O_5	**Phosphate**								
SnO_2	**Metal**								
SrO	**2**			2.51	[49]	0.32	1.02	-0.15	215
Cs_2O	**1**	12	1.88	3.23	[50]	0.10	0.04	-0.03	218
BaO	**2**	8	1.42	2.77	[51]	0.26	0.79	-0.16	220
K_2CO_3	**1**			3.02	[52]	0.11	0.54	-0.39	233
TiO_2	**4**	4	0.42	1.77	[53]	1.28	0.32	0.26	192
TiO_2	**4**	4	0.42	1.77	[53]	1.28	0.69	0.56	169
TiO_2	**4**	4	0.42	1.77	[53]	1.28	1.03	0.83	152
TiO_2	**4**	4	0.42	1.77	[53]	1.28	1.43	1.15	143
Reference								0	212
Al_2O_3	**3**	4	0.39	1.74	[16]	0.99			
CaO	**2**	7	1.06	2.41	[16]	0.34			
MgO	**2**	6	0.72	2.07	[16]	0.47			
SiO_2	**4**	4	0.26	1.61	[16]	1.54			
TiO_2	**4**	4	0.42	1.77	[53]	1.28			

4.2 Influence of minor elements on GGBS reactivity

SEM and XRD analysis showed that most added elements dissolved in the glass matrix. Yet, some elements showed an affinity for the small droplets of metallic iron typically present in industrial GGBS. Even though these elements were partitioned between metallic and glassy phases of the slag, the amount of metal was so small that the content of minor elements in the glassy phase measured by EDS was indistinguishable from bulk content measured by XRF. In an industrial setting however, with the presence of a large metallic phases, the partitioning would lead to lower glass contents. Only Sn and P were not detected at all by EDS in the glass. Sn formed metal droplets alone and together with iron. This was also confirmed by the presence of metallic Sn peaks in the XRD pattern of the SnO_2 modified GGBS sample (Figure 1). P appeared to form Ca-phosphates at the slag surface. Those elements will be excluded in the further discussion as they do not enter the slag glass structure. Also, these additions did not significantly modify the reactivity of the GGBS.

Additions of elements unambiguously known as network modifiers (K, Cs, Sr, Ba) had a positive effect on GGBS reactivity [51, 54]. All other elements had no or a negative effect. This suggests that the influence of additions is due to their stabilizing or destabilizing role in the glass network formation. The addition of network modifiers will likely increase the dissolution rate of the slag, thus lead to increased C-(A)-S-H formation and increased compressive strength [55]. In contrast network forming elements will stabilize the glass structure, and thus reduce the dissolution rate of the glass as was discussed for TiO_2 in section 4.1 [55].

A common concept that quantifies the effect of ions on network formation of oxide glasses is Dietzel's field strength [56]. Field strength is the simplified Coulomb's force of the ions in

glass and is defined as the charge of the metal cation divided by the square of the oxygen-metal cation bond length. Small highly charge cations thus have a high field strength and large single charged cations a low field strength. High field strength cations have the tendency to act as network formers thus stabilizing the glass structure, whereas low field strength cations act as network modifiers by compensating charges or by creating non bridging oxygens and thus destabilize the glass structure. Table 3 gives an overview of field strength of the elements used in this study. Coordination in slag like glasses is not available for many of the minor elements, and most of the data given in Table 3, are derived from aluminosilicate glasses of various composition. We assigned one single valence and coordination state to each element. Some elements, however, can be present in multiple sites and oxidation states in the glass [44, 48, 53].

To be able to estimate the effect of a certain addition on GGBS reactivity in blended cements, an index based on field strength of the element and the added amount is suggested here. The field strength of Mg was chosen to be used as a cutoff value between positive and negative impact of an addition. The underlying argument is that Mg is a relatively strong ion, but has been unambiguously reported to increase GGBS reactivity [8, 10, 13]. Stronger cations are expected to reinforce glass structure and decrease reactivity, whereas cations with lower field strength should destabilize the glass and increase reactivity. Based on this hypothesis, the field strength of Mg (Fs_{Mg}) is subtracted from the field strength of a given addition (Fs_M), giving a negative value for elements with lower field strength than Mg and a positive value for stronger cations. This value is then multiplied by the molar amount of the metal-oxide in the glass n and by the stochiometric factor x, of the metal from the oxide formula M_xO_y to give a field strength index (Eq. 1). For K and TiO_2 that were

already present in the reference slag, initial concentrations were subtracted from final concentrations to give the added amount.

$$Field\ strength\ index\ (FSI) = (Fs_M - Fs_{Mg}) * x * n(M_xO_y) \quad (1)$$

In Figure 7a the resulting FSI value is plotted against reaction heat. The good correlation (R^2 = 0.88) suggests that first order influences of minor element additions on reactivity are captured by the index.

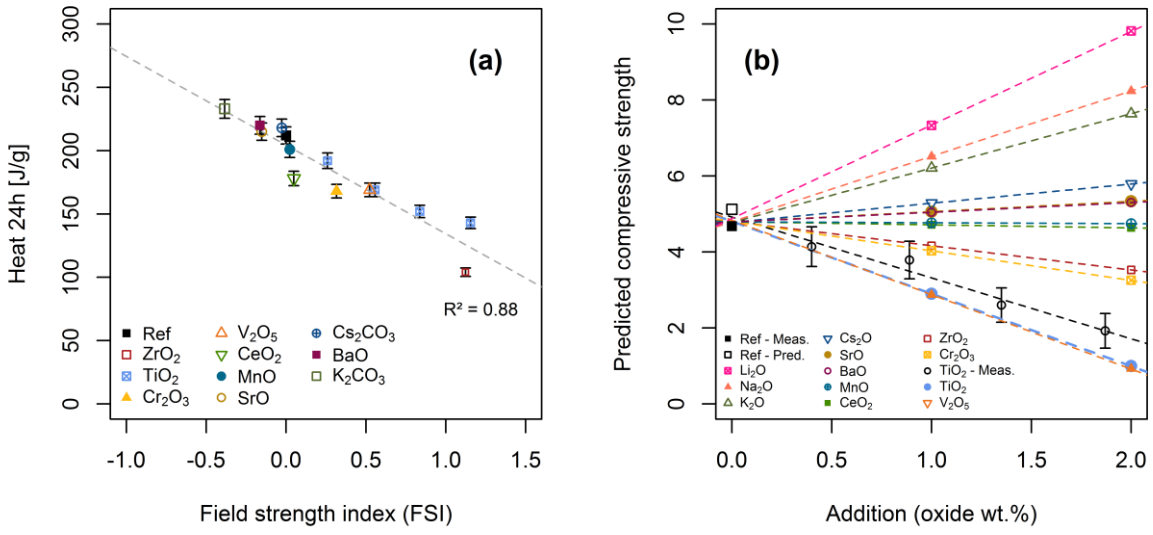

Figure 7. (a) Index values based on field strength and amount of added minor element plotted against the heat development during the R3-test. The grey dashed line is a linear regression. (b) Modeled compressive strength values based on the FSI index for the elements used in this study and the alkaline oxides Na_2O and Li_2O. R3 heat release was computed for oxide additions of 1 and 2 wt.% using the linear regression in (a) and converted to compressive strength using the regression shown in Figure 3a. Measured

compressive strength values of TiO_2 additions are added to the plot as well as expected compressive strength of the reference sample calculated from R3-test results.

The index value is a measure of the variation of glass stability due to some element addition. It indicates that if the glass stability is increased by the addition, the GGBS will be less reactive. This is likely due to decreased glass corrosion, which is a necessary step for the hydration reaction. In this case, the FSI value will be positive. On the other hand, if a weak ion is added to the slag and thus the glass is destabilized, reactivity will increase and the FSI will be negative. Leveling by the Mg field strength means that the effect is expected to be stronger (both positive and negative) if the field strength is further away from the Mg field strength. The effect appears to be proportional to the added amount, as was observed for TiO_2 additions. Minor deviations from the regression line are likely due to the fact that some elements can be present in multiple oxidation states and coordination numbers, that were not taken into account in the index.

Approaching GGBS reactivity only from a glass stability standpoint has the major drawback that it will not work when the component in question becomes major, so that it intervenes in the phase formation during hydration reaction. This is the case for example for Al_2O_3, which by the FSI would be considered detrimental for GGBS reactivity but actually is beneficial [8, 9, 13, 14]. This is likely due to modification of secondary phase assemblage due to the presence of Al_2O_3 and not increased glass corrosion. Nevertheless, the FSI gives a handy tool to estimate the effect of variations of minor element content on GGBS reactivity in blended cements.

Figure 7b shows modeled compressive strength for additions of various elements (in oxide wt.%) to the reference slag. These values were modelled using the FSI and field strength

values from Table 3. R3 heat release was then computed using the linear regression in Figure 7a and converted to compressive strength using the regression shown in Figure 3a. Besides the elements used in this study, Na_2O and Li_2O were added to the model using field strength of 0.18 and 0.26 eq./Å², respectively [51]. Measured compressive strength values from TiO_2 modifications are also displayed. Modeled values for TiO_2 additions are below measured ones but in the same order of magnitude and 95% confidence intervals of compressive strength measurements include modeled values in 2 of 4 points. This indicates that the model gives good estimates of reactivity but not accurate predictions.

Modeled values show the strongest positive effects on GGBS reactivity in Li_2O additions followed by Na_2O additions. This shows that the positive effect of small field strength of alkaline elements K and Cs is overcompensated by their high mass when reasoning in wt.%. The strongest negative effects on GGBS reactivity are calculated for Ti and V, due to their relatively high field strength and the relatively high molar fraction of the elements at equivalent addition level, due to their low atomic weight. This illustrates that Ti is the most important minor element for slag reactivity, as it has a strong impact by weight and is present in the weight percent range in industrial GGBS[8,39]. Other elements with strong negative impact by weight like V, Cr and Zr are commonly found only in the ppm range in modern slag[20].

5. Conclusion

TiO_2 additions have a strong negative effect on GGBS reactivity. A decrease of > 50% in 2 d compressive strength was observed on 75% GGBS standard mortars, when the TiO_2 content of the slag was increased by 1.9 wt.% (total 2.5 wt.%). This effect is persistent in time as > 40% lower 28 d compressive strength was observed for the same systems. The negative effect of Ti appears to be proportional to TiO_2 contents.

Loss in compressive strength was strongly correlated to R3-heat values measured by isothermal calorimetry. This showed that calorimetric test can be used to evaluate the impact of minor element additions on GGBS reactivity. Further calorimetric test showed that the addition of network modifiers (Ba, Cs, K, Sr,) increased GGBS reactivity. Other elements (namely Ce, Cr, V, Zr) had significant negative effects on GGBS reactivity. No demixing or nucleation occurred due to abovementioned element additions, so that those elements entered the glass matrix. P and Sn appeared to not enter the glass matrix and thus did not have significant effect on reactivity.

The effect on slag reactivity of a given element addition to GGBS depends on the field strength of the added element and its amount. The effect of a given addition can be estimated using a field strength index, based on the field strength of the added element with respect to the Mg field strength and the amount added to the slag.

Acknowledgements

This project has received funding from the Research Fund for Coal and Steel under grant agreement No 749809.

6. References

1. Ehrenberg A. Huttensand - Ein leistungsfahiger Baustoff mit Tradition und Zukunft - Teil 1. *Beton-Informationen*. 2006;46(4):35–63.
2. Matthes W, Vollpracht A, Villagrán Y, *et al.* Ground Granulated Blast-Furnace Slag. In: De Belie N, Soutsos M, Gruyaert E, eds. *Prop. Fresh Hardened Concr. Contain. Suppl. Cem. Mater.* Vol. 25. Cham: Springer International Publishing; 2018:1–53. https://doi.org/10.1007/978-3-319-70606-1_1
3. Bijen J. Benefits of slag and fly ash. *Constr Build Mater*. 1996;10(5):309–314. https://doi.org/10.1016/0950-0618(95)00014-3
4. Ehrenberg A. CO2 emissions and energy consumption of granulated blastfurnace slag. *Proc. Manuf. Process. Iron Steel Slags*. Vol. 3. Keyworth, UK: Euroslag publication; 2002:151–166.
5. Hogan F, Meusel J. Evaluation for Durability and Strength Development of a Ground Granulated Blast Furnace Slag. *Cem Concr Aggreg*. 1981;3(1):40. https://doi.org/10.1520/CCA10201J
6. Taylor HFW. Cement chemistry. 2nd ed. Thomas Telford Publishing; 1997 https://doi.org/10.1680/cc.25929
7. Van den Heede P, De Belie N. Environmental impact and life cycle assessment (LCA) of traditional and “green” concretes: Literature review and theoretical calculations. *Cem Concr Compos*. 2012;34(4):431–442. https://doi.org/10.1016/j.cemconcomp.2012.01.004
8. Blotevogel S, Ehrenberg A, Steger L, *et al.* Ability of the R3 test to evaluate differences in early age reactivity of 16 industrial ground granulated blast furnace slags (GGBS). *Cem Concr Res*. 2020;130:105998. https://doi.org/10.1016/j.cemconres.2020.105998
9. Ben Haha M, Lothenbach B, Le Saout G, Winnefeld F. Influence of slag chemistry on the hydration of alkali-activated blast-furnace slag — Part II: Effect of Al2O3. *Cem Concr Res*. 2012;42(1):74–83. https://doi.org/10.1016/j.cemconres.2011.08.005
10. Ben Haha M, Le Saout G, Winnefeld F, Lothenbach B. Influence of activator type on hydration kinetics, hydrate assemblage and microstructural development of alkali activated blast-furnace slags. *Cem Concr Res*. 2011;41(3):301–310. https://doi.org/10.1016/j.cemconres.2010.11.016
11. Gong K, White CE. Impact of chemical variability of ground granulated blast-furnace slag on the phase formation in alkali-activated slag pastes. *Cem Concr Res*. 2016;89:310–319. https://doi.org/10.1016/j.cemconres.2016.09.003
12. Smolczyk H-G. Zum Einfluß der Chemie des Hüttensands auf die Festigkeit von Hochofenzementen. 6th ed. *Zem - Kalk - Gips*. 1978;294–296.
13. Tänzer R, Buchwald A, Stephan D. Effect of slag chemistry on the hydration of alkali-activated blast-furnace slag. *Mater Struct*. 2015;48(3):629–641. https://doi.org/10.1617/s11527-014-0461-x
14. Wang PZ, Trettin R, Rudert V, Spaniol T. Influence of Al_2O_3 content on hydraulic reactivity of granulated blast-furnace slag, and the interaction between Al_2O_3 and CaO. *Adv Cem Res*. 2004;16(1):1–7. https://doi.org/10.1680/adcr.2004.16.1.1
15. Whittaker M, Zajac M, Ben Haha M, Bullerjahn F, Black L. The role of the alumina content of slag, plus the presence of additional sulfate on the hydration and microstructure of Portland cement-slag blends. *Cem Concr Res*. 2014;66:91–101. https://doi.org/10.1016/j.cemconres.2014.07.018
16. Shimoda K, Tobu Y, Kanehashi K, Nemoto T, Saito K. Total understanding of the local structures of an amorphous slag: Perspective from multi-nuclear (29Si, 27Al, 17O, 25Mg, and 43Ca) solid-state NMR. *J Non-Cryst Solids*. 2008;354(10–11):1036–1043. https://doi.org/10.1016/j.jnoncrysol.2007.08.010
17. Huang C, Behrman EC. Structure and properties of calcium aluminosilicate glasses. *J Non-Cryst Solids*. 1991;128(3):310–321. https://doi.org/10.1016/0022-3093(91)90468-L
18. Li C, Sun HH, Li LT. Glass Phase Structure of Blast Furnace Slag. *Adv Mater Res*. 2010;168–170:3–7. https://doi.org/10.4028/www.scientific.net/AMR.168-170.3

19. Piatak NM, Parsons MB, Seal RR. Characteristics and environmental aspects of slag: A review. *Appl Geochem*. 2015;57:236–266. https://doi.org/10.1016/j.apgeochem.2014.04.009
20. Proctor DM, Fehling KA, Shay EC, *et al.* Physical and Chemical Characteristics of Blast Furnace, Basic Oxygen Furnace, and Electric Arc Furnace Steel Industry Slags. *Environ Sci Technol*. 2000;34(8):1576–1582. https://doi.org/10.1021/es9906002
21. Ehrenberg A. Huttensand - Ein leistungsfahiger Baustoff mit Tradition und Zukunft - Teil 2. *Beton-Informationen*. 2006;46(5):67–95.
22. Wang PZ, Rudert V, Lang E, Trettin R. Influence of the TiO2 content on the reactivity of granulated blastfurnace slags. *Cem Int*. 2002;1:120–128.
23. Péra J, Ambroise J, Chabannet M. Properties of blast-furnace slags containing high amounts of manganese. *Cem Concr Res*. 1999;29(2):171–177. https://doi.org/10.1016/S0008-8846(98)00096-9
24. Rai A, Prabakar J, Raju CB, Morchalle RK. Metallurgical slag as a component in blended cement. *Constr Build Mater*. 2002;16(8):489–494. https://doi.org/10.1016/S0950-0618(02)00046-6
25. Criado M, Bernal SA, Garcia-Triñanes P, Provis JL. Influence of slag composition on the stability of steel in alkali-activated cementitious materials. *J Mater Sci*. 2018;53(7):5016–5035. https://doi.org/10.1007/s10853-017-1919-3
26. Januchta K, Bauchy M, Youngman RE, Rzoska SJ, Bockowski M, Smedskjaer MM. Modifier field strength effects on densification behavior and mechanical properties of alkali aluminoborate glasses. *Phys Rev Mater*. 2017;1(6):063603. https://doi.org/10.1103/PhysRevMaterials.1.063603
27. Thompson LM, Stebbins JF. Non-stoichiometric non-bridging oxygens and five-coordinated aluminum in alkaline earth aluminosilicate glasses: Effect of modifier cation size. *J Non-Cryst Solids*. 2012;358(15):1783–1789. https://doi.org/10.1016/j.jnoncrysol.2012.05.022
28. Thompson LM, Stebbins JF. Non-bridging oxygen and high-coordinated aluminum in metaluminous and peraluminous calcium and potassium aluminosilicate glasses: High-resolution 17O and 27Al MAS NMR results. *Am Mineral*. 2011;96(5–6):841–853. https://doi.org/10.2138/am.2011.3680
29. Zhang XH, Yue YL, Wu HT. Effects of cation field strength on structure and properties of boroaluminosilicate glasses. *Mater Res Innov*. 2013;17(3):212–217. https://doi.org/10.1179/1433075X12Y.0000000051
30. Das K, Raha S, Chakraborty D, Burhanuddin, Saheb Ali Sk. Effect of Nucleating Agents on the Crystallization and Microstructural Characteristics of Blast Furnace Slag Derived Glass-Ceramics. *Trans Indian Ceram Soc*. 2012;71(3):137–142. https://doi.org/10.1080/0371750X.2012.738482
31. Ding L, Ning W, Wang Q, Shi D, Luo L. Preparation and characterization of glass–ceramic foams from blast furnace slag and waste glass. *Mater Lett*. 2015;141:327–329. https://doi.org/10.1016/j.matlet.2014.11.122
32. Fredericci C, Pizani PS, Morelli MR. Crystallization of blast furnace slag glass melted in SnO2 crucible. *J Non-Cryst Solids*. 2007;353(44–46):4062–4065. https://doi.org/10.1016/j.jnoncrysol.2007.06.027
33. Kreidl N. Phase separation in glasses. *J Non-Cryst Solids*. 1991;129(1–3):1–11. https://doi.org/10.1016/0022-3093(91)90074-G
34. Li Z, Sun Y, Liu L, Wang X, Zhang Z. Enhancement of Rutile Formation by ZrO_2 Addition in Ti-bearing Blast Furnace Slags. *ISIJ Int*. 2015;55(7):1384–1389. https://doi.org/10.2355/isijinternational.55.1384
35. Sycheva GA. Nucleation of Crystals in Glass Based on Blast-Furnace Slag: Influence of Chemical Differentiation on the Process of Nucleation. *Glass Phys Chem*. 2019;45(1):19–28. https://doi.org/10.1134/S1087659619010127
36. Zhou H, Feng K, Chen C, Yan Z. Influence of CeO2 addition on the preparation of foamed glass-ceramics from high-titanium blast furnace slag. *Int J Miner Metall Mater*. 2018;25(6):689–695. https://doi.org/10.1007/s12613-018-1616-5

37. Avet F, Snellings R, Alujas Diaz A, Ben Haha M, Scrivener K. Development of a new rapid, relevant and reliable (R3) test method to evaluate the pozzolanic reactivity of calcined kaolinitic clays. *Cem Concr Res*. 2016;85:1–11. https://doi.org/10.1016/j.cemconres.2016.02.015
38. Li X, Snellings R, Antoni M, *et al.* Reactivity tests for supplementary cementitious materials: RILEM TC 267-TRM phase 1. *Mater Struct*. 2018;51(6). https://doi.org/10.1617/s11527-018-1269-x
39. Matthes W, Vollpracht A, Villagrán Y, *et al.* Ground Granulated Blast-Furnace Slag. In: De Belie N, Soutsos M, Gruyaert E, eds. *Prop. Fresh Hardened Concr. Contain. Suppl. Cem. Mater.* Vol. 25. Cham: Springer International Publishing; 2018:1–53. https://doi.org/10.1007/978-3-319-70606-1_1
40. Deubener J. Viscosity of Glass-Forming Melts. 1st ed. *P Richet Ed Encycl. Glass Sci. Technol. Hist. Cult.*, 1st ed. Wiley-American Ceramic Society; 2020
41. Pronina N, Krüger S, Bornhöft H, Deubener J, Ehrenberg A. Cooling history of a wet-granulated blast furnace slag (GBS). *J Non-Cryst Solids*. 2018;499:344–349. https://doi.org/10.1016/j.jnoncrysol.2018.07.054
42. EN 196-1. Methods of testing cement - Part 1: Determination of strengt. CEN n.d.
43. Steger L. Etude de l'accélération des ciments à haute teneur en laitier de haut-fourneau par du chlorure de calcium. PhD Thesis; Université Paul Sabatier; Toulouse; 2019
44. Cormier L, Dargaud O, Calas G, *et al.* Zr environment and nucleation role in aluminosilicate glasses. *Mater Chem Phys*. 2015;152:41–47. https://doi.org/10.1016/j.matchemphys.2014.12.008
45. Shannon RD. Revised Effective Ionic Radii and Systematic Studies of Interatomic Distances in Halides and Chalcogenides. *Acta Cryst*. 1976;A32:751–767.
46. Terczynska-Madej A, Cholewa-Kowalska K, Laczka M. The effect of silicate network modifiers on colour and electron spectra of transition metal ions. *Opt Mater*. 2010;32(11):1456–1462. https://doi.org/10.1016/j.optmat.2010.05.024
47. Li Y, Cao J, Xu B, Liang K. Spectroscopic Study of Optical Property and Structural State of Vanadium Ions in Lithium Aluminosilicate Glass-Ceramics. *Spectrosc Lett*. 2011;44(1):67–76. https://doi.org/10.1080/00387010903512855
48. Cicconi MR, Neuville DR, Blanc W, Lupi J-F, Vermillac M, de Ligny D. Cerium/aluminum correlation in aluminosilicate glasses and optical silica fiber preforms. *J Non-Cryst Solids*. 2017;475:85–95. https://doi.org/10.1016/j.jnoncrysol.2017.08.035
49. Kohn S, Charnock J, Henderson C, Greaves G. The structural environments of trace elements in dry and hydrous silicate glasses; a manganese and strontium K-edge X-ray absorption spectroscopic study. *Contrib Mineral Petrol*. 1990;105(3):359–368.
50. Minami T, Tokuda Y, Masai H, *et al.* Structural analysis of alkali cations in mixed alkali silicate glasses by ^{23}Na and ^{133}Cs MAS NMR. *J Asian Ceram Soc*. 2014;2(4):333–338. https://doi.org/10.1016/j.jascer.2014.07.001
51. Brown GE, Farges F, Calas G. X-Ray scattering and X-rayspectroscopy studies of silicate melts. *Struct. Dyn. Prop. Silic. Melts*. Vol. 32. Washington D.C.: Mineralogical Society of America; 1995:317–410.
52. Jackson W, Brown Jr G, Ponader C. X-ray absorption study of the potassium coordination environment in glasses from the NaAlSi3O8-KAlSi3O8 binary: Structural implications for the mixed-alkali effect. *J Non-Cryst Solids*. 1987;93(2–3):311–322.
53. Farges F, Brown GE, Navrotsky A, Gan H, Rehr JJ. Coordination chemistry of Ti(IV) in silicate glasses and melts: II. Glasses at ambient temperature and pressure. *Geochim Cosmochim Acta*. 1996;60(16):3039–3053. https://doi.org/10.1016/0016-7037(96)00145-7
54. Zachariasen WH. THE ATOMIC ARRANGEMENT IN GLASS. *J Am Chem Soc*. 1932;54(10):3841–3851. https://doi.org/10.1021/ja01349a006
55. Bunker BC. Molecular mechanisms for corrosion of silica and silicate glasses. *J Non-Cryst Solids*. 1994;179:300–308. https://doi.org/10.1016/0022-3093(94)90708-0

56. Dietzel A. Die Kationenfeldstärke und ihre Beziehung zu Entglasungsvorgängen, zur Verbindungsbildung und zu den Schmelzpunkten von Silikaten. *Zeit Elektrochem*. 1942;48:9–23.